# Composition Dependence of Electronic, Elastic, and Polarization Properties of Wurtzite InxGa1-xN and CdxZn1-xO Ternary Alloys

**Abdesamed BENBEDRA**
Université de Mostaganem
**Said MESKINE** ( said.meskine@univ-mosta.dz )
Université de Mostaganem
**Hamza ABBASSA**
Université de Mostaganem
**El Habib ABBES**
Université de Mostaganem
**Abdelkader BOUKORTT**
Université de Mostaganem

**Research Article**

**Keywords:** Wurtzite crystals, Ternary alloys, FP-LAPW, Berry phase, Electric polarization

**Posted Date:** November 3rd, 2021

**DOI:** https://doi.org/10.21203/rs.3.rs-1009180/v1

# Composition dependence of electronic, elastic, and polarization properties of wurtzite $In_xGa_{1-x}N$ and $Cd_xZn_{1-x}O$ ternary alloys

Abdesamed Benbedra, Said Meskine*, Hamza Abbassa, El Habib Abbes, and Abdelkader Boukortt

Laboratoire d'Elaboration et Caractérisation Physico Mécanique et Métallurgique des Matériaux (ECP3M), Université *Abdelhamid Ibn Badis*, Route Natoinale N°11, Kharouba, 27000 Mostaganem, Algeria
*Corresponding author: said.meskine@univ-mosta.dz

**Abstract**

We report the results of density functional theory calculations of several properties of wurtzite-structured InGaN and CdZnO alloys. It is shown that the investigated properties, including the internal parameter, bandgap, mechanical moduli, and electric polarization are nonlinear functions of alloy composition, as they deviate from the linear behavior predicted by Vegard's law. Based on these results, InGaN and CdZnO are materials whose properties can be tuned via In and Cd concentrations. The spontaneous and piezoelectric polarizations considerably affect the properties of alloys-based devices due to the huge electric fields that build up at the heteroineterfaces. In this work we propose a method of controlling such fields by employing the composition dependence of the total polarization. We support this proposal by showing, in the case of InGaN, that an optimal alloy composition can be found that effectively reduces the polarization-induced electric fields, thereby improving the efficiency of optoelectronic applications.

**Key words:** Wurtzite crystals, Ternary alloys, FP-LAPW, Berry phase, Electric polarization.

## I. Introduction

Over the past two decades, group III-nitrides and II-oxides materials have found applications in a wide range of domains, including optoelectronics, microelectronics, and electromechanical devices. Among these, the field of optoelectronics is the one that has allowed the emergence of the most promising technologies, namely light emitting diodes, laser diodes, and photovoltaic solar cells [1-4]. This is mainly due to the fact that most of these materials are semiconductors with direct bandgaps [1,2], which prefer radiative transitions. The wurtzite structure in which the III-N and II-O compounds crystallize is non-centrosymmetric, i.e., it lacks an inversion center. As such, these materials exhibit both spontaneous and strain-induced piezoelectric polarization [5,6], making them attractive candidates for applications which require efficient electromechanical coupling [7,8].

Despite this technological importance, there are still some issues that limit the range of applications and/or the performance of the associated devices. For example, the bandgap values of pure binaries are limited, which causes a problem when looking at a particular wavelength not compatible with the gap of any binary. Furthermore, and in the context of lighting applications, it is now established that electric polarization tends to reduce the optical efficiency [9,10], it is therefore desirable to find ways to minimize this effect in order to enhance the said efficiency. Solving these and other problems may require the use of alloys (solid solutions), where one can adjust the value of the alloy composition to obtain the desired bandgap and polarization [11]. This method of alloying different materials can be applied to control other physical properties as well. Having a varying bandgap energy, any alloy can be thought of as a

quantum well: a two dimensional heterostructure which is the basic building block of all the active optoelectronic devices mentioned above [12,13].

III-nitrides and II-oxides binaries and their alloys have been studied intensively. In this paper, we choose to investigate the structural, electronic, mechanical, and polarization properties of two wurtzite ternary alloys: indium gallium nitride $In_xGa_{1-x}N$ and cadmium zinc oxide $Cd_xZn_{1-x}O$. This amounts to calculating lattice parameters, optical bandgaps, elastic constants, and electric polarizations. The study of the effect of alloy chemical composition on these quantities is the central theme of this article. Here, the word "composition" refers to the quantity $x$ of the incorporated In and Cd atoms. The main finding is that almost all the investigated properties have a nonlinear behavior with the alloy composition. Due to this, we use the quadratic modification of Vegard's law throughout the present work to interpret the results of our calculations and to determine the respective bowing parameters. We show that $In_xGa_{1-x}N$ and $Cd_xZn_{1-x}O$ semiconductors can emit and absorb light wavelengths that span the visible spectrum and beyond. Also, we demonstrate that for the technologically relevant case of $In_xGa_{1-x}N$, a suitable choice of alloy composition can lead to an effective reduction of the strong polarization fields across this alloy, thus allowing the development of high-efficiency optoelectronic $In_xGa_{1-x}N$ -based devices.

## II. Alloys structure

Since we are interested in the properties of alloys, a careful identification of their equilibrium structure is needed. $In_xGa_{1-x}N$ and $Cd_xZn_{1-x}O$ (henceforth labeled InGaN and CdZnO for brevity) are mixtures of GaN-InN and ZnO- CdO, respectively. They are formed by replacing a number of Ga (Zn) atoms by a corresponding number of In (Cd) atoms. The constituent binaries crystallize in the hexagonal wurtzite structure [1,2]. This structure is completely defined by an in-plane $a$ and out-of-plane $c$ lattice constants, in addition to an internal parameter $u$ that measures the bond length parallel to the $c$-axis [5]. The only exception is CdO, which prefers the cubic rocksalt structure [14]. Given that GaN and InN share the wurtzite phase, their alloy InGaN is stable in this structure for any In concentration. However, this is not the case with CdZnO, since the wurtzite phase of ZnO is expected to convert to the rocksalt phase of CdO upon increasing the Cd concentration; such a phenomenon is known as phase separation [15]. One has to conduct a thermodynamic study based on the concept of the mixing enthalpy to find the concentration for which the wurtzite-to-rocksalt transition takes place [15,16]. This is outside the scope of the present work. Experimental reports indicate that CdZnO can retain the wurtzite structure up to 7% of Cd content [17]. In our study we assume the latter statement to hold for the entire range of alloy composition, with the hope that future experiments will succeed in growing CdZnO alloys with much higher Cd contents. Another point to consider is the existence of ordered and random structures of alloys [18], depending on the growth conditions; herein, we restrict ourselves to ordered systems.

In order to model the structure of the two alloys we use wurtzite supercells, and we work with five concentrations $x$ (molar fractions) of In and Cd: $x$=0, 0.25, 0.5, 0.75 and 1. Each value of $x$ corresponds to a specific number of In and Cd atoms. As an example, for $x$=0.25 the supercell contains one atom of In/Cd, in this case the alloys may be designated as $In_{0.25}Ga0_{.75}N$

and $Cd_{0.25}Zn_{0.75}O$. The parent compounds correspond to concentrations 0 and 1. The adopted supercells of both InGaN and CdZnO are shown in figure 1 for each concentration $x$.

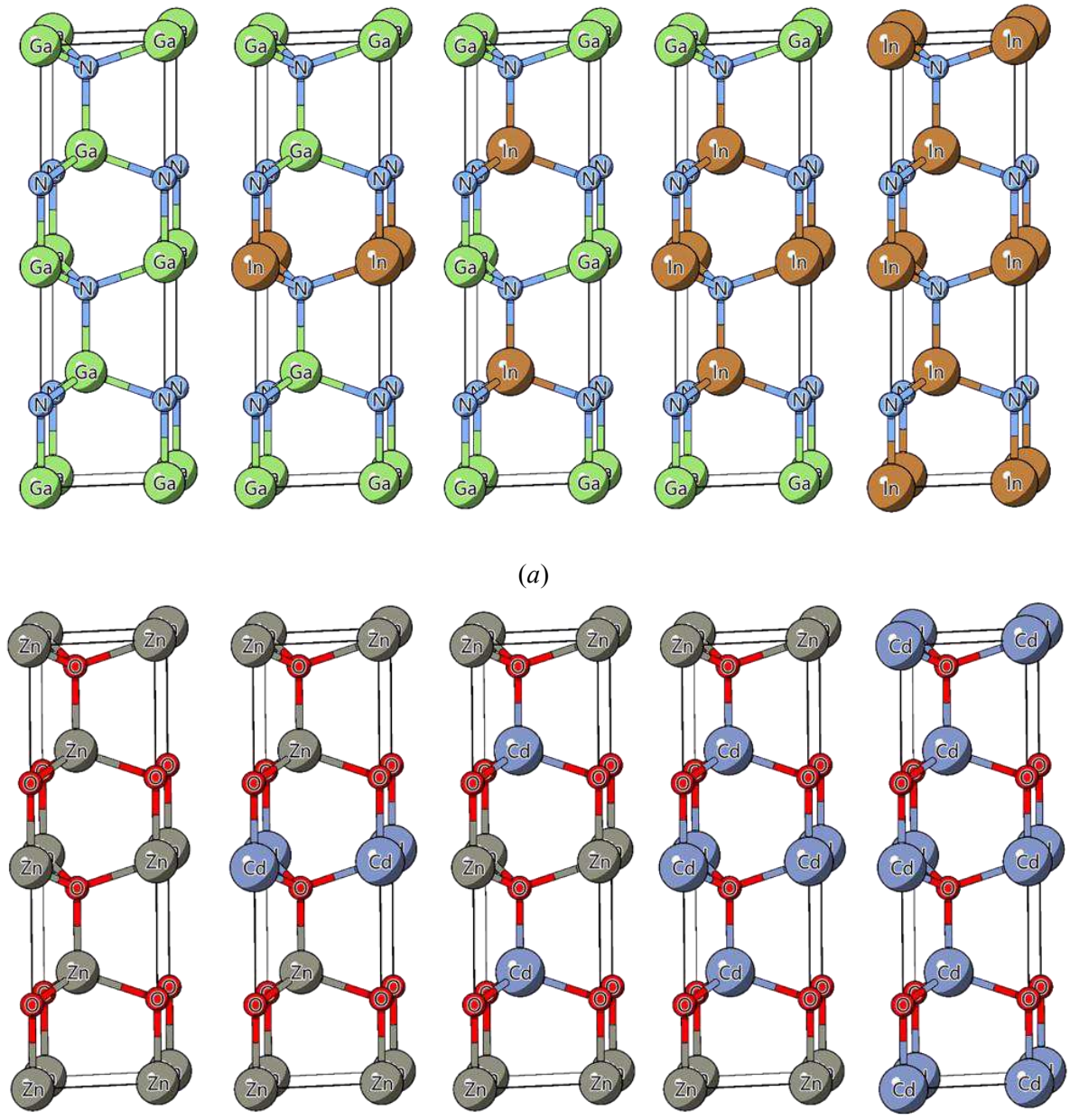


**Figure 1** Crystalline structure of wurtzite (*a*) InGaN and (*b*) CdZnO alloys for concentrations $0 \leq x \leq 1$. The supercells are constructed by extending the unit cell in the *c*-direction.

## III. Methods and computational details

The physical properties of InGaN and CdZnO ternary alloys are calculated using the full potential linearized augmented plane wave (FP-LAPW) method [19,20] within the framework of density functional theory [21]. We use the WIEN2k package [22] with the generalized gradient approximation (GGA) to treat the exchange-correlation interactions [23]. The modified Becke-Johnson (mBJ) approach is chosen for dealing with electronic properties [24], since it was successfully applied for studying such properties in many materials. There are several

parameters that need to be adjusted to carry out the first-principles computations. In the spirit of the FP-LAPW method, we expand the solutions of the Khon-Sham equation [25] on two different basis sets: localized atomic-like orbitals with a cutoff $l_{max}$=10 and plane waves with a cutoff $R_{MT}$ $K_{max}$=7, where $l_{max}$ is the maximum angular momentum, $R_{MT}$ is the radius of the smallest muffin-tin sphere, and $K_{max}$ is the norm of the largest wave vector. The first Brillouin zone is sampled uniformly using a 7×7×7 mesh, which corresponds to ~500 k-points. We set the energy that separates core and valence electrons to be equal to -6 Ry. The radii of muffin-tin spheres centered at individual atoms are chosen as follows: 2, 1.5, 2.1, 2.05, 1.6, and 2.15 Bohr for Ga, N, In, Zn, O and Cd, respectively.

The structural equilibrium parameters and electronic properties are studied by means of standard total energy calculation. The convergence criteria on the energy and electric charge are of the order of 0.1 mRy and 0.001$e$. To determine the internal parameter of the wurtzite structure, we carry out a relaxation process by minimizing the Hellman-Feynman forces acting on atomic sites [26], such that the convergence condition on the forces is 0.5 mRy/Bohr. As for elastic properties, we resort to an energy-strain method implemented in the software IRelast [27]. Finally, the code BerryPI is used to calculate polarization properties [28], which is the only realization of the Berry phase theory of electric polarization in WIEN2k.

The main goal of this study is to investigate the degree to which the properties of InGaN and CdZnO can be affected by their composition. In doing do, we use the so-called Vegard's law. The latter is an empirical role which states that the values of physical properties in an alloy interpolates linearly between the limiting values determined by the parent compounds [29]. For a generic property P and a ternary alloy $A_xB_{1-x}C$, where BC and AC are the parent compounds, Vegard's law is written as

$$P_{A_xB_{1-x}C} = xP_{AC} + (1-x)P_{BC}. \quad (1)$$

However, most properties are found to deviate from this linear behavior, making the predictions of Vegard's law not accurate enough [29]. To a fairly good approximation, the compositional nonlinearities (curvatures) are described by a quadratic model via the introduction of the bowing parameter $b$ [30]

$$P_{A_xB_{1-x}C} = xP_{AC} + (1-x)P_{BC} - bx(1-x). \quad (2)$$

Once the bowing parameter is known, the value of P can be predicted for any concentration.

### Data Availability

The data that support the findings of this study are available from the corresponding author upon reasonable request.

## IV. Results and discussion

### IV.1 Structural properties

In order to determine the ground-state structural properties of InGaN and CdZnO in the wurtzite phase, a self-consistent calculation of the total energy for several volumes is performed. The computations are initialized and repeated until the convergence criteria are verified. In figure 2, we plot the variations of the total energy of both alloys as a function of cell volume for the

whole range of In and Cd concentration ($0 \leq x \leq 1$). The E(V) curves as well as the structural parameters are obtained by fitting the calculated data by the Murnaghan equation of state [31].

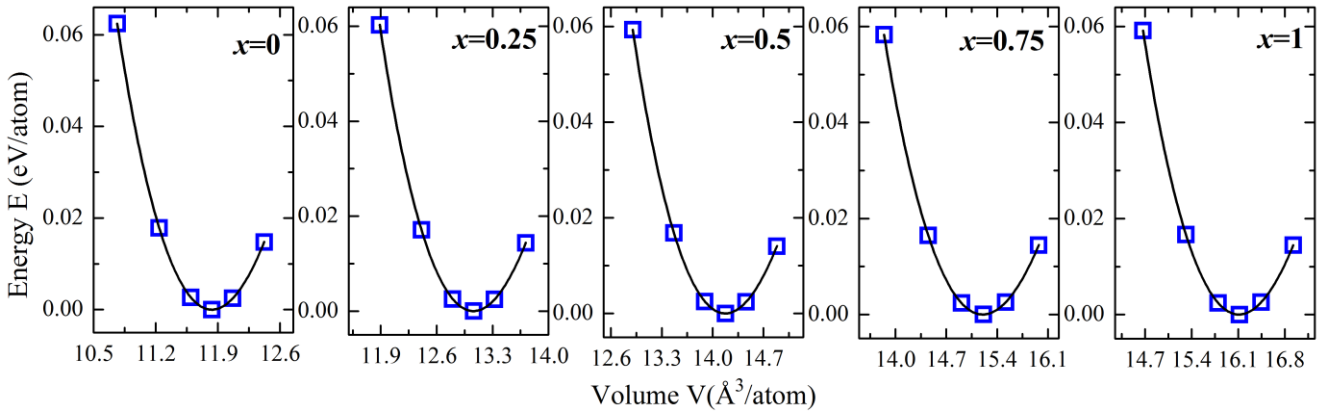


(*a*)

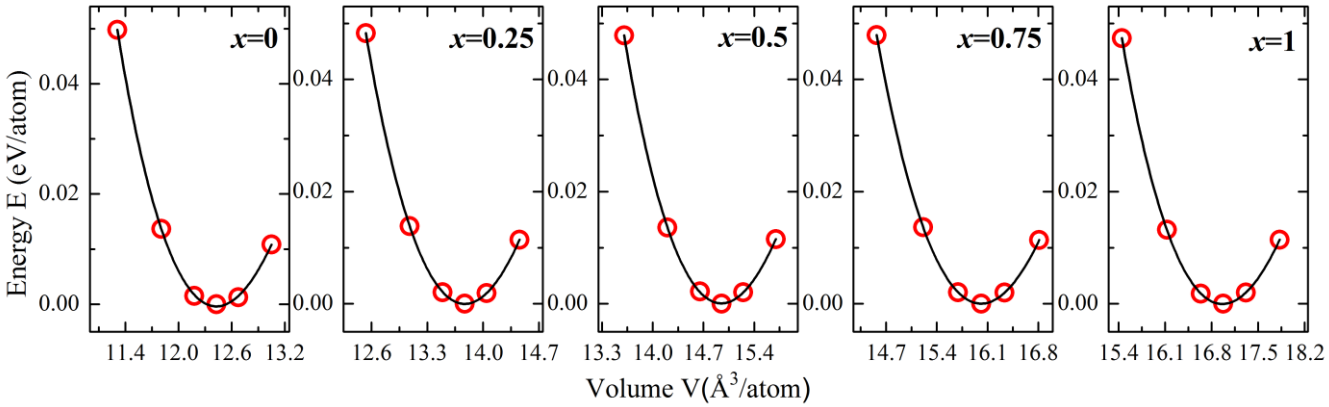


(*b*)

**Figure 2** Total energy E versus volume V for (*a*) InGaN and (*b*) CdZnO in the wurtzite structure. For each alloy concentration, the energy is shifted by the minimal value. The curves are fits of the Murnaghan equation.

Since the crystalline structure is hexagonal, the volume depends on two parameters: *a* and *c*. Hence, the energy is also evaluated for different values of *c*/*a* to determine the optimal ratio. The results of this calculation, including the E(*c*/*a*) curves, are not presented. The different sizes of Ga (Zn) and In (Cd) atoms results in deviations of bond lengths [12]. It is therefore necessary to fully relax the internal parameters to find their new equilibrium values. As indicated previously, this is done by minimizing the applied atomic forces. InGaN and CdZnO are usually grown as layers on GaN and ZnO substrates [32], so that one speaks of InGaN/GaN and CdZnO/ZnO quantum wells. Such configurations are characterized by residual strains at the interface [33], i.e. perpendicular to the direction of growth, invariably chosen to be the [0001] direction (*c*-axis) [34]. The origin of these strains is the difference in the in-plane lattice parameter *a* of different layers [33]. To quantify this effect we calculate the in-plane lattice mismatch $\varepsilon_a$ via

$$\varepsilon_a = \frac{a_{GaN} - a_{InGaN}}{a_{GaN}}, \qquad (3)$$

| | InGaN | | | | | CdZnO | | | | |
|---|---|---|---|---|---|---|---|---|---|---|
| $x$ | $a$ (Å) | $c$ (Å) | $u$ | B (GPa) | $\varepsilon_a$(%) | $a$ (Å) | $c$ (Å) | $u$ | B (GPa) | $\varepsilon_a$(%) |
| 0 | 3.226 | 5.252 | 0.377 | 175.192 | 0 | 3.293 | 5.294 | 0.380 | 128.526 | 0 |
| 0.25 | 3.337 | 5.419 | 0.376 | 153.360 | -3.441 | 3.412 | 5.468 | 0.379 | 116.715 | -3.614 |
| 0.5 | 3.430 | 5.564 | 0.353 | 138.504 | -6.324 | 3.508 | 5.612 | 0.352 | 106.398 | -6.529 |
| 0.75 | 3.512 | 5.694 | 0.355 | 129.548 | -8.865 | 3.589 | 5.739 | 0.353 | 99.066 | -8.989 |
| 1 | 3.584 | 5.793 | 0.379 | 122.859 | -11.097 | 3.659 | 5.851 | 0.382 | 92.593 | -11.114 |

**Table 1** Calculated lattice constants $a$ and $c$, internal parameter $u$, bulk modulus B, and $a$-lattice mismatch (strain) for different compositions of wurtzite InGaN and CdZnO alloys within the GGA approximation.

where $a_{InGaN}$ and $a_{GaN}$ refer to the $a$ lattice constants of the epitaxial layer (InGaN) and the substrate (GaN), respectively. A similar expression holds for CdZnO/ZnO. The results of the structural parameters, namely the lattice constants $a$ and $c$, the internal parameter $u$, the zero-pressure bulk modulus B are grouped in table 1 for every concentration $x$. Also included is the lattice mismatch just mentioned. Our calculated lattice parameters of the end materials GaN, InN and ZnO agree well with previous experimental data [2,35]. For CdO, we compare our results to those reported in Ref. [14]: while the values of $a$ are close to each other, the values of $c$ and $u$ show a level of disagreement. The negative values of the mismatch indicates that the corresponding strains are compressive.

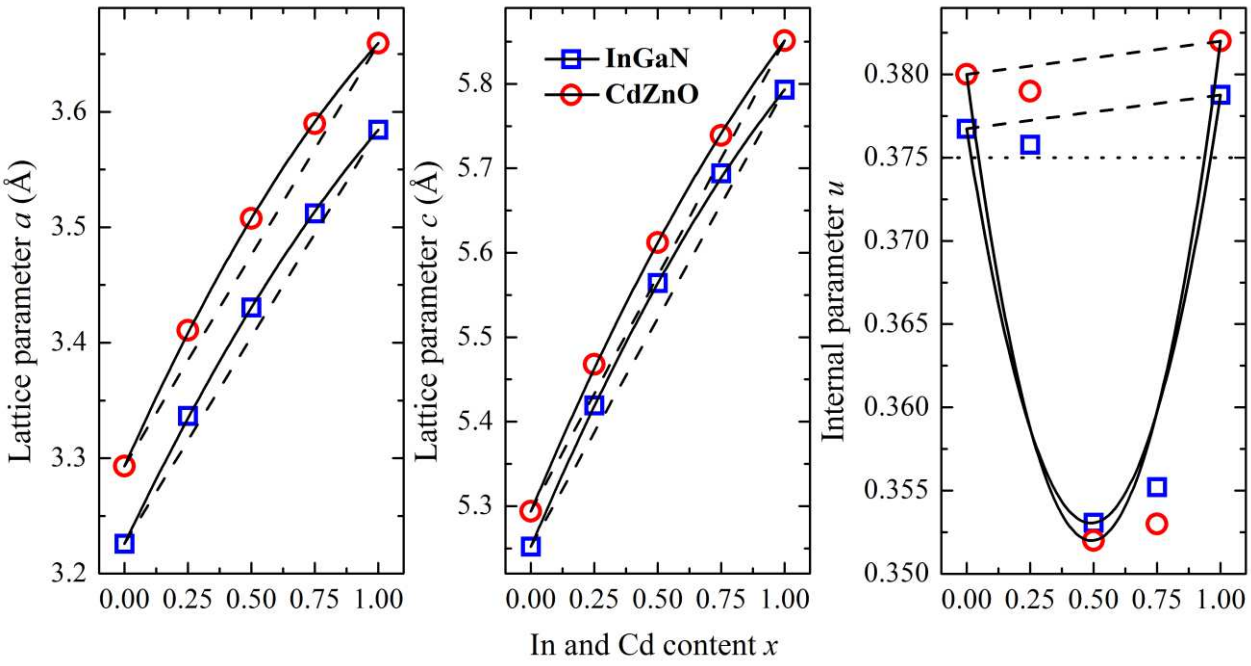


**Figure 3** Lattice constants $a$ and $c$ and internal parameter $u$ as a function alloy concentration $x$ for wurtzite InGaN (blue squares) and CdZnO (red circles). Solid curves are obtained by adjusting the value of the bowing parameter $b$, and dashed straight lines represent the predictions of Vegard's law. The dotted horizontal line in $u(x)$ is the value of $u$ in the ideal wurtzite structure.

Figure 3 shows the variations of the lattice constants $a$ and $c$ and the internal parameter $u$ as a function of composition. In this figure, open blue squares (open red circles) are the calculated values for InGaN (CdZnO); dashed lines are Vegrad-law predictions while solid lines

are fits of Eq. 2. We note, for the two alloys, that the lattice constants increase monotonically as the concentration increases from 0 to 1. This is explained by the addition of the large In (Cd) atoms and their substitution with the small Ga (Zn) ones, which induces an extension of the crystal. Our results indicate that $a$ and $c$ parameters deviate slightly from Vegard's law. In contrast, the internal parameter exhibits a large bowing. It can be observed that for both alloys the internal parameter is smaller than the ideal value $u$=0.375 at the concentrations 0.5 and 0.75. Following Eq.2, we use a quadratic interpolation to determine the dependence of the lattice parameters $a$, $c$ and $u$ on the alloy concentration $x$. The resulting expressions are

$$\begin{aligned} a_{\mathrm{InGaN}} &= 3.584x + 3.226(1-x) + 0.101x(1-x) \\ c_{\mathrm{InGaN}} &= 5.793x + 5.252(1-x) + 0.165x(1-x) \\ u_{\mathrm{InGaN}} &= 0.379x + 0.377(1-x) - 0.098x(1-x) \\ a_{\mathrm{CdZnO}} &= 3.659x + 3.293(1-x) + 0.126x(1-x) \\ c_{\mathrm{CdZnO}} &= 5.851x + 5.294(1-x) + 0.158x(1-x) \\ u_{\mathrm{CdZnO}} &= 0.382x + 0.380(1-x) - 0.116x(1-x). \end{aligned} \tag{4}$$

The numerical factor in the third term of Eqs. 4 represents the bowing parameters. The nonlinearity of $u$ is described by almost the same bowing parameter $b$=0.1. As shown in figure 4 ($a$), the bulk modulus B is found to decrease with increasing concentration, suggesting that the introduction of In and Cd atoms into InGaN and CdZnO makes them more compressible. We approximate the variation of B($x$) by the following quadratic equation

$$\begin{aligned} B_{\mathrm{InGaN}} &= 122.859x + 175.192(1-x) - 41.203x(1-x) \\ B_{\mathrm{CdZnO}} &= 92.593x + 128.526(1-x) - 16.646x(1-x). \end{aligned} \tag{5}$$

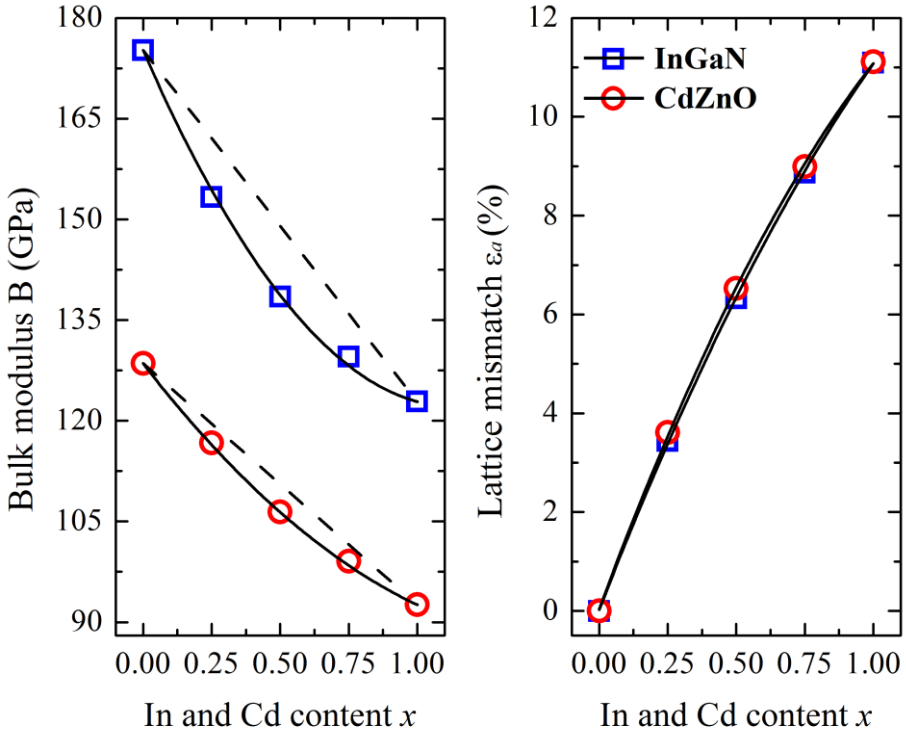


($a$) ($b$)

**Figure 4** ($a$) Bulk modulus B and ($b$) the magnitude of in-plane lattice mismatch $\varepsilon_a$ as a function of alloy concentration $x$ for wurtzite InGaN and CdZnO.

We now address the lattice mismatch in the basal plane between InGaN (CdZnO) and GaN (ZnO) layers. Figure 4 (*b*) presents the evolution of the mismatch (in absolute value) with alloy composition. It can be seen that the mismatch significantly increases as the In and Cd molar fraction increases, which means that InGaN and CdZnO are strained structures by construction. The mismatch-induced strains are as high as 11% for the two alloys, thus resulting in the formation of a large defect density at the interface [36]. The impact of the lattice mismatch on the optical characteristics will be discussed in the next subsection.

## IV.2 Electronic properties

We use the FP-LAPW method to calculate the band structure of the ternaries InGaN and CdZnO in the wurtzite structure. The GGA and mBJ approximations are both employed to model the exchange-correlation potential. The band structures calculated by the mBJ approach at the points of high symmetry are shown in figure 5 for various compositions of InGaN and CdZnO.

By analyzing these curves, the first remark is the existence of an energy gap (forbidden band), which confirms the semiconducting nature of InGaN and CdZnO. It is also observed that the maximum of the valence band and the minimum of the conduction band coincide at the point Γ for all concentrations. Consequently, our alloys are direct gap semiconductors (Γ-Γ) over the entire interval of $x$. Table 2 gives the results of the bandgap energies calculated by GGA and mBJ and the corresponding wavelengths for each concentration, together with the experimental data of the parent materials.

| $x$ | InGaN | | | | CdZnO | | | |
|---|---|---|---|---|---|---|---|---|
| | $E_g\ (eV)$ | | | $\lambda\ (nm)$ | $E_g\ (eV)$ | | | $\lambda\ (nm)$ |
| | GGA | mBJ | Exp. | | GGA | mBJ | Exp. | |
| 0 | 1.683 | 2.966 | 3.5[a] | 418.49 | 0.780 | 2.698 | 3.4[b] | 460.06 |
| 0.25 | 0.619 | 1.469 | - | 844.96 | 0.215 | 1.961 | - | 632.98 |
| 0.5 | 0.14 | 1.291 | - | 961.46 | 0.092 | 2.042 | - | 607.86 |
| 0.75 | 0 | 0.818 | - | 1517.42 | 0 | 1.714 | - | 724.18 |
| 1 | 0 | 0.751 | 0.7[a] | 1652.80 | 0 | 1.798 | 2.4[c] | 690.35 |

[a] Ref. [1], [b] Ref. [2], [c] Ref. [37]

**Table 2** Bandgap energy $E_g$ and corresponding wavelengths $\lambda$ of InGaN and CdZnO alloys in the wurtzite phase for different concentrations. The gaps are computed at the GGA and mBJ levels.

It is evident that the gap values obtained by GGA are severely underestimated compared to those found experimentally. In particular, in the case of ZnO the discrepancy between theory and experiment is about 76%, and both InN and CdO are predicted to be metals. It is well established that the GGA functional fails to reproduce the band structure of semiconductors by underestimating their bandgap [38], often by several electronvolts. To surmount this difficulty we use the mBJ method, which provides much more accurate and reliable results for the bandgap [39]. This fact is shown by our results (table 2), where the gaps obtained by mBJ are found in good agreement with the experimental ones.

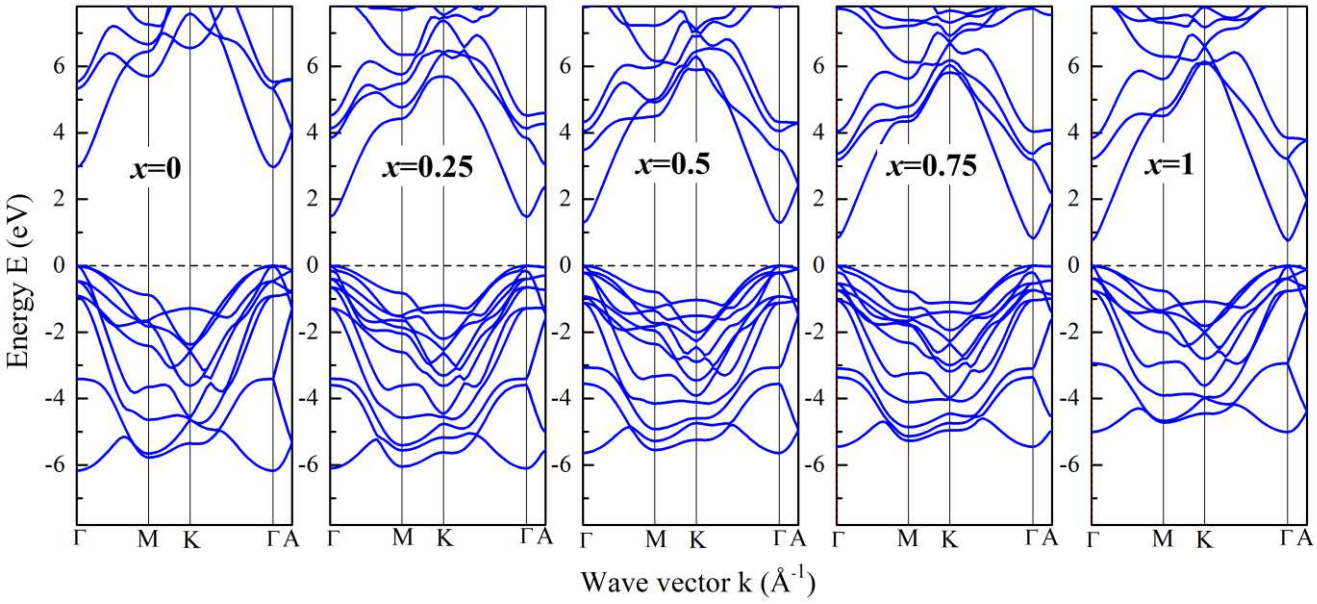


(*a*)

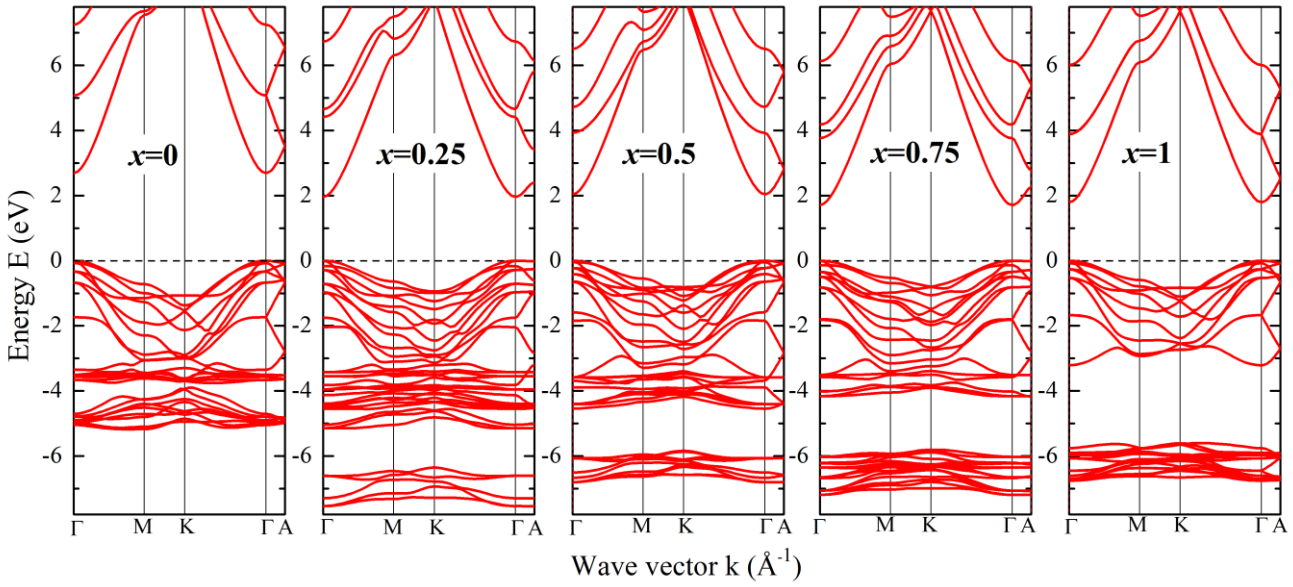


(*b*)

**Figure 5** Band structures for various concentrations of wurtzite (*a*) InGaN and (*b*) CdZnO ternaries obtained using the mBJ approximation. The origin of energies is the Fermi level (the dashed line).

For the design of alloys-based optoelectronic devices, it is imperative to know the behavior of the fundamental bandgap with composition. Hence, the variations of the mBJ bandgap as a function of alloy concentration are depicted in figure 6. The incorporated In and Cd atoms lead to a reduction in the energy gap of both alloys. The optical bandgap does not follow Vegard's law; instead, its compositional dependence departs form linearity. Fitting the calculated data using a second order polynomial yields bowing parameters equal to 2.79 and 1.65 eV for InGaN and CdZnO, respectively. These values of *b* are within the range of the experimental values reported in the literature [40,41]. The bandgap as a function of composition is then given by [42]

$$E_{g(\mathrm{InGaN})} = 0.751x + 2.966(1-x) - 2.796x(1-x)$$
$$E_{g(\mathrm{CdZnO})} = 1.798x + 2.698(1-x) - 1.648x(1-x). \quad (6)$$

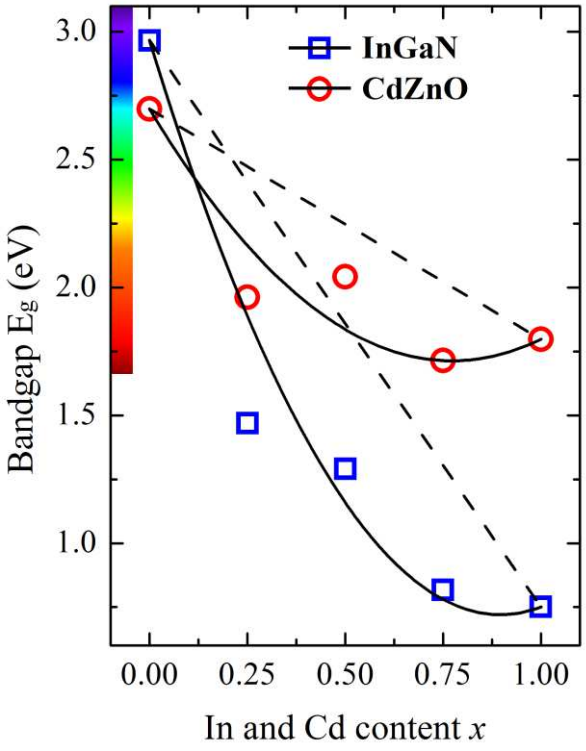


**Figure 6** Bandgap $E_g$ as a function of alloy composition $x$ for InGaN and CdZnO in the wurtzite structure. The values of the gap are those obtained by the mBJ approach. The colored strip represents the visible spectrum, which is comprised between 3.2 (380) and 1.7 eV (750 nm).

Based on these results, we point out that InGaN and CdZnO alloys have a set of bandgaps which covers the visible part of the electromagnetic spectrum. As such, one can access any wavelength in between simply by tuning the In and Cd content. InGaN and CdZnO have been already exploited in the fabrication of violet and blue light-emitting diodes [43,44], and further inspection of figure 6 indicates the possibility to extend the application of InGaN to longer wavelengths (near infrared). In practice, however, the large lattice mismatch of GaN-InN and ZnO-CdO result in several challenges that impose severe limitations on the experimentally achievable alloys [33]. As a consequence, the range of possible wavelengths is reduced significantly from the one expected by the bandgaps. Since the mismatch and the associated strains increase with the alloy composition, the most challenging issue is the growth of high-quality InGaN and CdZnO heterostructures with high In and Cd content [45]. Indeed, the amount of In that can be incorporated into InGaN is about 28% ($x$=0.28) [46]. In the case of CdZnO, a lower Cd content of 12% has been reported [44]. InGaN and CdZnO with higher concentrations results in poor crystal quality due to the formation of structural defects (dislocations) [47]. Furthermore, these defects stimulate non-radiative transitions, which attenuates the light emission and degrades the performance of quantum well devices [48]. One possible strategy to deal with this issue is to introduce a small amount of elements with a lower atomic radius, such as B and Be, to form quaternary alloys. This technique was applied for

cubic InGaN and found to lead to a reduction of the lattice mismatch between the GaN substrate and the InGaN active layers [49].

### IV.3 Elastic and Mechanical properties

In this part, we investigate the elastic and mechanical properties of InGaN and CdZnO. Having hexagonal symmetry, these ternary alloys are characterized by five independent elastic constants: $C_{11}$, $C_{12}$, $C_{13}$, $C_{33}$, and $C_{44}$ [50], the determination of which relies on calculating the total energy at fixed values of appropriate mechanical deformations [51]. The calculated elastic constants are summarized in table 3 for different alloy concentrations.

| | InGaN | | | | | CdZnO | | | | |
|---|---|---|---|---|---|---|---|---|---|---|
| $x$ | 0 | 0.25 | 0.5 | 0.75 | 1 | 0 | 0.25 | 0.5 | 0.75 | 1 |
| $C_{11}$ | 327.411 | 258.853 | 222.646 | 201.917 | 204.438 | 221.094 | 151.709 | 139.311 | 132.689 | 129.402 |
| $C_{12}$ | 113.227 | 88.166 | 84.322 | 90.026 | 93.274 | 75.134 | 88.166 | 74.929 | 77.015 | 92.799 |
| $C_{13}$ | 82.287 | 87.044 | 76.199 | 75.016 | 61.859 | 69.902 | 95.670 | 55.660 | 82.232 | 45.106 |
| $C_{33}$ | 355.296 | 306.798 | 267.745 | 235.180 | 205.011 | 271.559 | 237.378 | 131.732 | 134.033 | 175.219 |
| $C_{44}$ | 91.373 | 71.509 | 57.150 | 52.326 | 49.579 | 44.389 | 35.114 | 27.116 | 24.977 | 19.987 |

**Table 3** Calculated elastic constants $C_{ij}$ (in GPa) of wurtzite InGaN and CdZnO alloys for $0 \leq x \leq 1$.

The elastic constants are doubly interesting. On the one hand, they provide access to several elastic properties that describe the mechanical behavior of materials. On the other hand, they make it possible to verify the mechanical stability of the system via the Born stability criteria. For a hexagonal crystal, these criteria are as follows [50]

$$C_{11} > |C_{12}|; 2C_{13}^2 < C_{33}(C_{11} + C_{12}); C_{44} > 0. \quad (7)$$

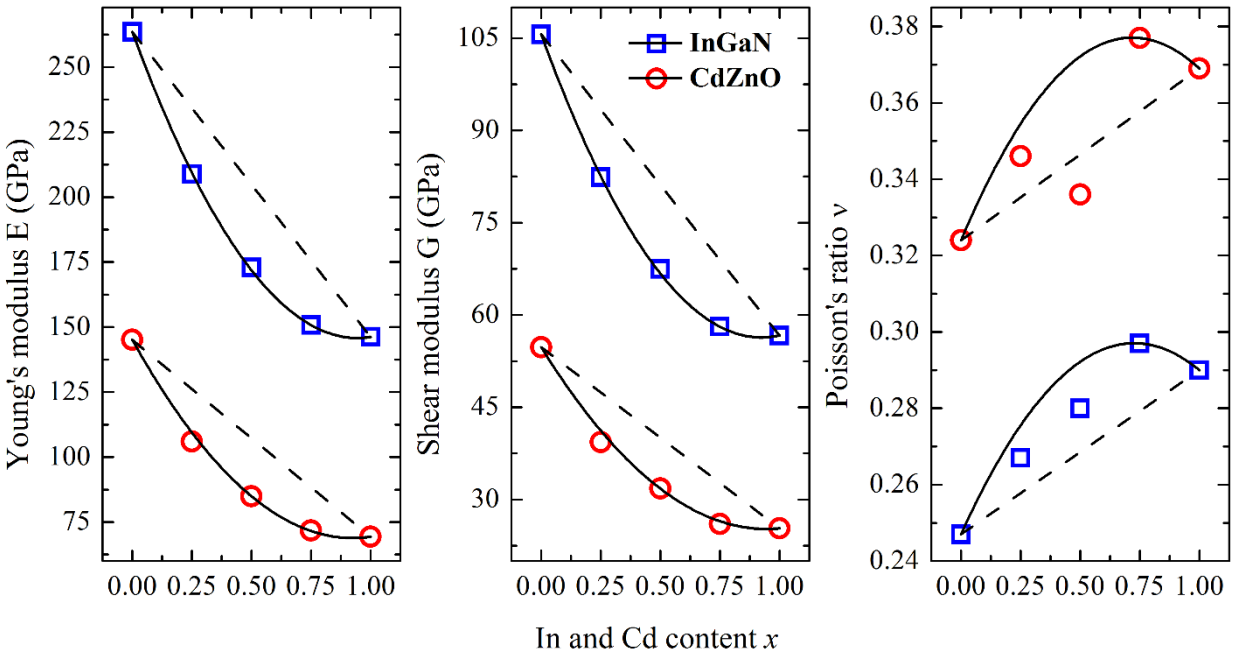


**Figure 7** Young modulus E, shear modulus G, and Poisson's ratio $\nu$ as a function of In and Cd content $x$ for wurtzite InGaN and CdZnO alloys.

According to our numerical data, the elastic constants satisfy the stability conditions, which implies that InGaN and CdZnO alloys are mechanically stable. Using the elastic constants, we compute many important mechanical parameters, including Bulk modulus (B), shear modulus (G), Pugh's ratio (B/G), Young modulus (E), Poisson's coefficient $\nu$, anisotropy index (A), Debye temperature $\theta_D$, and sound velocity (v). These quantities are listed in table 4. The current B values differ slightly from those found by the Murnaghan equation. The calculated B/G ratios are greater than the threshold value of 1.75, which classifies InGaN and ZnO as ductile materials (except GaN for which B/G=1.65) [52]. Notice that $\nu$ is always positive, and its values fall in the expected theoretical interval [-1,0.5] [53]. Finally, the values of A are around unity regardless of the alloy composition, confirming the mechanical isotropic character of the systems under study [54].

| | InGaN | | | | | CdZnO | | | | |
|---|---|---|---|---|---|---|---|---|---|---|
| $x$ | 0 | 0.25 | 0.5 | 0.75 | 1 | 0 | 0.25 | 0.5 | 0.75 | 1 |
| B | 173.968 | 149.492 | 131.547 | 124.267 | 116.211 | 137.893 | 115.375 | 86.669 | 98.008 | 88.892 |
| G | 105.626 | 82.392 | 67.502 | 58.104 | 56.664 | 54.771 | 39.325 | 31.778 | 26.046 | 25.323 |
| B/G | 1.647 | 1.814 | 1.949 | 2.139 | 2.051 | 2.518 | 2.934 | 2.727 | 3.763 | 3.510 |
| E | 263.541 | 208.813 | 172.927 | 150.807 | 146.223 | 145.101 | 105.938 | 84.951 | 71.779 | 69.380 |
| $\nu$ | 0.247 | 0.267 | 0.280 | 0.297 | 0.290 | 0.324 | 0.346 | 0.336 | 0.377 | 0.369 |
| A | 0.853 | 0.838 | 0.826 | 0.935 | 0.892 | 0.608 | 1.105 | 0.842 | 0.897 | 1.092 |
| $\theta_D$ | 614.829 | 519.453 | 451.401 | 403.731 | 384.198 | 457.102 | 368.514 | 315.673 | 276.231 | 262.196 |
| v | 4705.64 | 4108.79 | 3669.26 | 3359.27 | 3259.27 | 3556.33 | 2952.70 | 2593.76 | 2331.80 | 2262.72 |

**Table 4** Mechanical properties of different compositions of wurtzite InGaN and CdZnO ternary alloys. The properties are: bulk modulus B (in GPa), shear modulus G (in GPa), Pugh's ratio B/G, Young's modulus E (in GPa), Poisson's coefficient $\nu$, mechanical anisotropy index A, Debye temperature $\theta_D$ (in K), and sound velocity v (in m/s).

Figure 7 shows the variations of the Young's modulus, shear modulus, and Poisson's ratio as a function of concentration. A moderate bowing is observed. To provide a predictive model we fit the computed data to quadratic polynomials

$$\begin{aligned} E_{\mathrm{InGaN}} &= 146.2x + 263.5(1-x) - 131.9x(1-x) \\ G_{\mathrm{InGaN}} &= 56.66x + 105.63(1-x) - 57.6x(1-x) \\ \nu_{\mathrm{InGaN}} &= 0.29x + 0.247(1-x) + 0.0947x(1-x) \\ E_{\mathrm{CdZnO}} &= 69.4x + 145.1(1-x) - 89.2x(1-x) \\ G_{\mathrm{CdZnO}} &= 25.3x + 54.77(1-x) - 33.1x(1-x) \\ \nu_{\mathrm{CdZnO}} &= 0.369x + 0.324(1-x) + 0.10x(1-x). \end{aligned} \tag{8}$$

The curves in figure 7 show that the moduli E and G decrease with increasing alloy concentration, meaning that by adding In and Cd, these ternary compounds become less resistant to shear stress and uniaxial pressure. From a microscopic point of view, elastic moduli are related to chemical bonds [55], and any decrease in their values reflects the weakness of the bonding between the constituent elements. Conversely, the Poisson's ratio increases with composition. We conclude that the Poisson effect, i.e. the elongation of the material perpendicular to the direction of the applied uniaxial stress [53], becomes more important as In and Cd content increases.

## IV.3 Polarization properties

The study of electric polarization is carried out by the Berry phase method [56-58]. It should be noted that the absolute value of polarization is not defined, only the difference in polarization has a physical meaning and corresponds to measurable quantities [57,58]. Such a difference manifests itself as a geometric quantum phase of the crystal wavefunctions known as the Berry phase [59]. This approach has been used successfully to study the polarization in many materials, including pure binaries and their ternary and quaternary alloys. Here, we report a similar calculation for InGaN and CdZnO alloys crystallizing in the wurtzite structure.

In alloy-based heterostructures, the mismatch strains discussed above contribute in a piezoelectric polarization $P_{pz}$ [34], and even in the absence of such strains, the system has a spontaneous polarization $P_{sp}$. So in general the total polarization, $P_{tot}$, at the interface is the sum of spontaneous and piezoelectric contributions [18].

### IV.3.1 Spontaneous polarization

The spontaneous polarization is the value of polarization at equilibrium. It results from an intrinsic reduction in symmetry within the crystal [58], such as the existence of a nonideal atomic position, i.e., an internal parameter. Indeed, the spontaneous polarization is found to depend sensitively on internal structural parameters [60]. In the Berry phase scheme, the spontaneous polarization is defined as a difference in polarization between two different structures of the same material: a non-centrosymmetric structure and its reference centrosymmetric counterpart [58]

$$P_{sp} = P_{nc} - P_c, \tag{9}$$

where $P_{nc}$ and $P_c$ are, respectively, the polarization of the non-centrosymmetric and centrosymmetric structure. For wurtzite crystals, the structure that serves as a reference turns out to be the ideal wurtzite phase, in which the internal parameter $u$ and the $c/a$-ratio are fixed to their ideal values: $u = 3/8$ and $c/a = \sqrt{8/3}$ [30]. The ideal wurtzite structure is equivalent to cubic zincblende [14], and is centrosymmetric because the four tetrahedral bonds are equivalent; that is to say, the bond lengths and the interbond angles between the first nearest neighbors are equal [30].

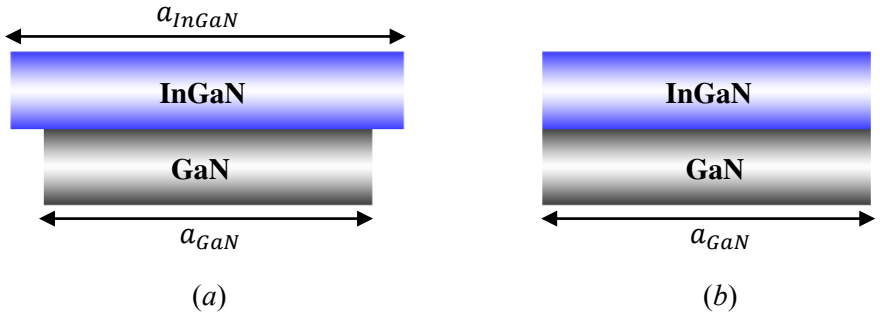


**Figure 8** Schematics of (*a*) a free-strain and (*b*) strained (lattice-matched) structures of InGaN/GaN quantum well. While the former is used to calculate only the spontaneous polarization, the latter is used to access both spontaneous and piezoelectric polarizations (i.e., total polarization).

Calculating the spontaneous polarization requires the elimination of the residual strains. To do this we consider a free-strain structure, where the in-plane lattice parameters *a* of the substrate GaN (ZnO) and the active layer InGaN (CdZnO) are not similar as illustrated in figure 8 (*a*). The lattice parameters that we use (*a*,*c*,*u*) are those listed in table 1. Once the structures are prepared, we evaluate the spontaneous polarization with the Berry phase technique for each In and Cd content. In table 5 we report the results of this calculation. It can be seen that InGaN and CdZnO have a large spontaneous polarization. The horizontal *x*- and *y*-components of the polarization vector are negligible, meaning that the spontaneous polarization is parallel to the *z*-axis (or *c*-axis). This is explained by the intrinsic asymmetry of the bonding being along this specific direction. The polarization quantum *ec*/V is found to be in the range from 1.78 to 1.38 C/m². Comparing this to our calculated polarizations, we conclude that our values are unambiguously well-defined [5,58]. Regarding the sign of the spontaneous polarization, it is negative over the entire concentration range for CdZnO. With reference of figures 1 and 8, the polarization vector is vertical and directed from top to bottom. However, for InGaN, a sign reversal is observed: the spontaneous polarization becomes positive for the intermediate molar fractions of In (*x*=0.25, 0.5 and 0.75). This sign reversal reflects the fact that the polarization vector changes its orientation from - *c* to + *c*.

| *x* | InGaN | | CdZnO | |
|---|---|---|---|---|
| | $P_{sp}$ (C/m²) | | $P_{sp}$ (C/m²) | |
| | Our work | Other calc. | Our work | Other calc. |
| 0 | -0.01433 | -0.029[a] | -0.02719 | -0.050[b] |
| 0.25 | 0.00557 | - | -0.02008 | - |
| 0,5 | 0.03003 | - | -0.01204 | - |
| 0,75 | 0.00283 | - | -0.02457 | - |
| 1 | -0.02476 | -0.032[a] | -0.02979 | -0.106[c] |

[a] Ref. [5], [b] Ref. [61], [c] Ref. [14]

**Table 5** Berry phase results of spontaneous polarization $P_{sp}$ of wurtzite InGaN and CdZnO for various alloy compositions. The values of $P_{sp}$ are referenced to the ideal wurtzite structure.

The results of the polarization for the pure binaries (*x*=0 and *x*=1) are in only relative agreement with prior theoretical works. For the nitrides GaN and InN, we suspect that the discrepancy is due to the use of another reference geometry, one that is different from the ideal wurtzite structure. Also, note that the experimental figure of GaN, which is -0.022 C/m² [62], is intermediate between our result and that of the literature. As for ZnO, our value of the spontaneous polarization is smaller than the one obtained by other authors, but using the experimental lattice parameters our value becomes very close to theirs. Our result for CdO differs significantly from the only theoretical prediction of Ref. [14]. Part of this discrepancy owes to the disagreement of the lattice parameters reported previously. To prove this, we constrain CdO to have the lattice parameters of Ref. [14] (*a*=3.6 Å, *c*=5.58 Å, and *u*=0.391); we obtain a spontaneous polarization equal to -0.0785 C/m².

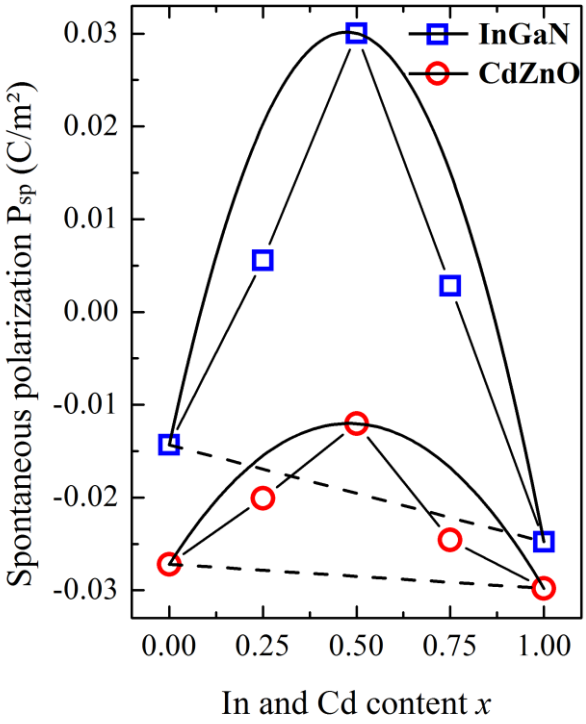


**Figure 9** Spontaneous polarization $P_{sp}$ as a function of alloy composition $x$ for InGaN and CdZnO in the wurtzite phase. The lines connecting the data points are a guide to the eye.

To show how the spontaneous polarization behaves in our ternary alloys, we present in figure 9 its variations as a function if In and Cd concentration. We find that the spontaneous polarization displays a significant degree of upward bowing, making our computed values very different for the predictions of Vegard's law. This is to be expected because the internal parameter is a nonlinear function of alloy composition. Using the theoretical approach followed throughout this work, the spontaneous polarization of the ternary alloys can be expressed to second order in the concentration as

$$\begin{aligned} P_{sp\ (\mathrm{InGaN})} &= -0.02476x - 0.01433(1-x) + 0.1983x(1-x) \\ P_{sp\ (\mathrm{CdZnO})} &= -0.02979x - 0.02719(1-x) + 0.0658x(1-x). \end{aligned} \qquad (10)$$

The bowing parameter of InGaN is -0.198 C/m², to be compared with another calculation -0.038 C/m² [18]. We report for CdZnO a bowing parameter of -0.0658 C/m². The polarization nonlinearity is attributed to three main factors [18]: (i) the macroscopic deformation due to the binaries having different volumes, (ii) the microscopic strain due to the different sizes of the constituent atoms, and (iii) the disordered effect due to the random distribution of the elements within the structure. Since we only consider ordered alloys, the nonlinear behavior is entirely structural in nature [due to factors (i) and (ii)].

### IV.3.2 Total polarization

In the following, we focus on the important case of InGaN. To access the total polarization of this alloy, the mismatch strains must be taken into account. This is done by constraining the in-plane lattice parameter of the alloy to the underlying substrate (i.e., $a_{InGaN} = a_{GaN}$), and allowing the out-of-plane lattice parameter $c$ and the internal parameter $u$ to fully relax as the

strain is applied [32,18]. This process of enforcing the equality of the lattice constants is called epitaxial matching [see figure 8 (*b*)], and the resulting structure simulates the case of a wurtzite alloy epitaxially grown on an unstrained substrate along the polar direction [0001]. The relaxation of the lattice parameter $c$ accounts for the Poisson effect [14], and amounts to calculating for each biaxial strain the total energy of the strained structure over a grid of values of $c$. Because this process is computationally expensive, we relies on another method taking advantage of the calculated Poisson's coefficient presented previously. The latter is defined as $\nu = -\varepsilon_c/\varepsilon_a$ where $\varepsilon_a$ is the epitaxial compressive strain in the $a$-direction and $\varepsilon_c$ is the ensuing elongation along the $c$-direction [53]. Then the parameter $c$ is determined by $c = c_0(1 + \varepsilon_c)$, where $c_0$ is the equilibrium zero-strain lattice constant. The definition of the Poisson's coefficient is valid in the elastic linear regime, where the stains are fairly small; for much greater strains, such as those employed in this study, the use of the Poisson's coefficient may be inappropriate. However, we argue that this method still provides us with a rough estimate of the elongation of the parameter $c$ due to the in-plane strain.

| $x$ | $a$ (Å) | $c$ (Å) | $u$ | $P_{tot}$ (C/m²) |
|---|---|---|---|---|
| 0 | 3.226 | 5.252 | 0.377 | -0.0143 |
| 0.25 | 3.226 | 5.469 | 0.369 | 0.00702 |
| 0.5 | 3.226 | 5.663 | 0.337 | 0.0519 |
| 0.75 | 3.226 | 5.844 | 0.332 | 0.0789 |

**Table 6** Calculated lattice constant $c$, internal parameter $u$, and total electric polarization $P_{tot}$ of strained wurtzite InGaN alloy for compositions $0 \leq x \leq 0.75$. The lattice constant $a$ is fixed to the calculated value of GaN, and the parameters $c$ and $u$ are relaxed.

The piezoelectric term of the total polarization is determined by the same kind of computation used for the spontaneous term. The results of the strained lattice parameters $a$, $c$, and $u$, as well as the total polarization $P_{tot}$ of InGaN epitaxially grown on GaN are given in table 6, for the concentration range $0 \leq x \leq 0.75$. Recall that the lattice parameter $a$ is identical by construction for all concentrations. With increasing alloy composition (and hence with increasing in-plane strain), the lattice parameter $c$ increases while the internal parameter $u$ decreases. The total polarization is plotted in figure 10 as a function of In composition. We identify two main points. First, there is a monotonous quasi-linear increase of the total polarization with alloy composition. Second, the total polarization resulted to be numerically zero at the concentration $x$=0.14, which means that the spontaneous and piezoelectric components cancel each other out.

One of the main problems that are encountered when dealing with nitride-based optoelectronic devices is the existence of built-in electrostatic fields [30,63,64]. These fields can be very large (of the order of 1 MV/cm for InGaN/GaN), and originate from gradients in total polarization at the interface of heterostructure layers. We refer to Ref. [63] for more details including the formulas that relate the total polarization and the resulting fields in different situations. From an experimental standpoint, one can confirm the existence of such fields via measurements of the quantum-confined Stark effect [65], which reduces radiative recombination rates through the separation of electrons and holes [66,67]. This effect is the physical origin of the efficiency droop of light emitters. In solar cells, the internal fields acts as a barrier that opposes the carrier collection [68,69], and therefore leads to a dramatic reduction in the light-generated current. In order to overcome this problem, composition engineering in

alloys has been proposed as a route toward suppression (or screening) of the strong electric fields present in III-N quantum well devices [63,67,70]. That being said, the fact that the total polarization vanishes in InGaN for some In concentration indicates that the structure at this composition is free of electric fields. Also, it is a key point to notice that the zero-field In concentration ($x$=0.14) is lesser than the current experimental critical limit 0.28, making it possible for quantum wells to be built and employed in the fabrication of high-performance optoelectronic devices.

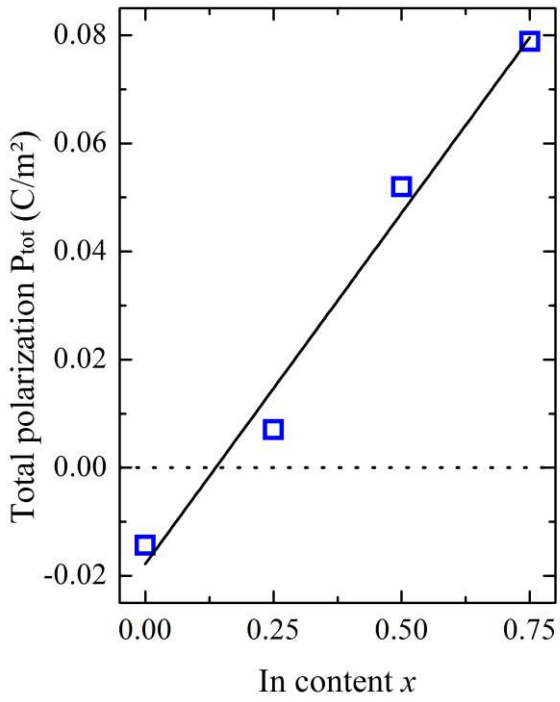


**Figure 10** Total polarization $P_{tot}$ as a function of In content $x$ for InGaN alloy in the wurtzite phase. The curve results from a linear regression of the calculated data: $P_{tot} = ax + b$, where $a$=0.1298 C/m² and $b$=-0.0178 C/m². The dotted horizontal line indicates zero-polarization $P_{tot}$=0 C/m².

## V. Conclusion

In summary, we have presented a theoretical study of the structure, bandgap, elasticity, and electric polarization of wurtzite ternary alloys. Because of their importance in the field of optoelectronics, InGaN and CdZnO were the main focus of this study. We have demonstrated the feasibility of composition engineering of different physical properties of alloys. This is particularly important in controlling the emitted wavelengths and the internal electric fields in heterostructures where wurtzite nitrides and oxides are employed. The investigated properties exhibit a nonlinear dependence on alloy concentration $x$, leading to the conclusion that Vegard's law is the exception rather than the rule. The nonlinearity is the largest for the two related quantities: the internal parameter and the spontaneous polarization. We have also shown that it is possible to reduce and even cancel the built-in electric fields within heterostructure systems. This is achieved by taking advantage of the strain and composition dependence of the total polarization. Specifically, a carful choice of the alloy composition can lead to a zero net polarization, and hence to a zero field. For strained InGaN alloy, the In content that gives a null total polarization was found to be equal to $x$=0.14 (14%). Our hope is that this field control

method will improve the design and operation of quantum well optoelectronic devices. As a final point, our numerical results may serve as inputs in theoretical simulations, for example in quantifying the effects of different material parameters and in interpreting the results of future experiments.

## References


[1] I. Vurgaftman and J. R. Meyer, J. Appl. Phys., 94:3675 (2003).
[2] Ü. Özgüra, Ya. I. Alivov, C. Liu, A. Teke, M. A. Reshchikov, S. Doğan, V. Avrutin, S.-J. Cho, and H. Morkoç, J. Appl. Phys., 98, 041301 (2005).
[3] S. A. Kazazis, E. Papadomanolaki and E. Iliopoulos, IEEE J. Photov. 8, 118 (2018).
[4] G. Siddharth, R. Singh, V. Garg, B. S. Sengar, M. Das, B. Mandal, M. T. Htay, M. Gupta, and S. Mukherjee, IEEE Trans. Electron Devices 67 (2020).
[5] F. Bernardini, V. Fiorentini, and D. Vanderbilt, Phys. Rev. B 56, R10024 (1997).
[6] Y. Noel, C.M. Zicovich-Wilson, B. Civalleri, P.D. Arco, and R.Dovesi, Phys. Rev. B 65, 014111 (2001).
[7] K. Shimada, Jpn. J. Appl. Phys. 45 L358 (2006).
[8] N. L. Marana, S. M. Casassa, and J. R. Sambrano, chemphys, 10.1016 (2017).
[9] P. Waltereit, O. Brandt, A. Trampert, H. T. Grahn, J. Menniger,M. Ramsteiner, M. Reiche, and K. H. Ploog, Nature 406, 406 (2000).
[10] E. Kioupakis, Q. Yan, and C.G.V. Walle, Appl. Phys. Lett. 101, 231107 (2012).
[11] V. Gedam, A. Pansari, and B. K. Sahoo, J. Electron. Mater., (2015).
[12] L. Dong and S. P. Alpay, J Mater Sci, 47 (2012).
[13] E. O. Odoh and A. S. Njapba, Adv Phys Theor Appl, 46 (2015).
[14] P. Gopal and N. A. Spaldin, J. Elec. Mater. 35 (2006).
[15] C. Hoglund, J. Birch, B. Alling, J. Bare~no, Z. Czig´any, P. O. Persson, G. Wingqvist, A. Zukauskait_e, and L. Hultman, J. Appl. Phys. 107, 123515 (2010).
[16] S. Manna, K. R. Talley, P. Gorai, J. Mangum, A. Zakutayev, G. L. Brennecka, V. Stevanovia, and C. V. Ciobanu, Phys. Rev. Applied 9, 034026 (2018).
[17] T. Makino, Y. Segawa, M. Kawasaki, A. Ohtomo, R. Shiroki, K. Tamura, T. Yasuda, and H. Koinuma, Appl. Phys. Lett. 78, 1237 (2001).
[18] F. Bernardini and V. Fiorentini, Phys. Rev. B 64, 085207 (2001).
[19] J. C. Slater, Phys. Rev. 51, 846 (1937).
[20] G. K. H. Madsen, P. Blaha, K. Schwarz, E. Sjöstedt, and L. Nordström, Phys. Rev. B 64, 195134 (2001)
[21] P. Hohenberg and W. Kohn, Phys. Rev. 136, B864 (1964).
[22] P. Blaha, K. Schwarz, F. Tran, R. Laskowski, G. K. H. Madsen and L. D. Marks, J. Chem. Phys. 152, 074101 (2020).
[23] J. P. Perdew, K. Burke, and M. Ernzerhof, Phys. Rev. Lett. 77, 3865 (1996).
[24] A. D. Becke and E. R. Johnson, J. Chem. Phys. 124, 221101 (2006).
[25] W. Kohn and L. J. Sham, Phys. Rev. 140, A1133 (1965).
[26] P. Pulay, Mol. Phys. 17, 197 (1969).
[27] M. Jamal, M. Bilal, Iftikhar Ahmad, and S. Jalali-Asadabadi, J. Alloys Compd. 735, 569 (2018).
[28] S. J. Ahmed, J. Kivinen, B. Zaporzan, L. Curiel, S. Pichardo, and O. Rubel, Comput. Phys. Commun. 184, 647 (2013).

[29] S. T. Murphy, A. Chroneos, C. Jiang, U. Schwingenschlögl, and R. W. Grimes, Phys. Rev. B, 82, 073201 (2010).
[30] O. Ambacher, J. Majewski, C. Miskys, A. Link, M. Hermann, M. Eickhoff, M. Stutzmann,F. Bernardini, V. Fiorentini and V. Tilak, B. Schaff, and L. F. Eastman, J. Phys.: Condens. Matter 14 3399 (2002).
[31] F. D. Murnaghan, Proc. Natl. Acad. Sci. USA 30, 5390 (1944).
[32] A. Malashevich and D. Vanderbilt, Phys. Rev. B 75, 045106 (2007).
[33] L. K. Teles, J. Furthmüller, L. M. R. Scolfaro, J. R. Leite, and F. Bechstedt, Phys. Rev. B 62, 2475 (2000).
[34] T. Paskova, phys. stat. sol. (b), 245:1011 (2008).
[35] K. Lawniczak-Jablonska, T. Suski, I. Gorczyca, N. E. Christensen, K. E. Attenkofer, R. C. C. Perera, E. M. Gullikson, J. H. Underwood, D. L. Ederer, and Z. Liliental Weber, Phys. Rev. B 61, 16623 (2000).
[36] H. K. Cho, J. Y. Lee, G. M. Yang, and C. S. Kim, Appl. Phys. Lett., 79:215 (2001).
[37] F. P. Koffyberg, Phys. Rev. B 13, 4470 (1976).
[38] J. Heyd, J. E. Peralta, G. E. Scuseria, and R. L. Martin, J. Chem. Phys. 123, 174101 (2005).
[39] F. Tran, J. Doumont, L. Kalantari, A. W. Huran, M. A. L. Marques, and P. Blaha, J. Appl. Phys. 126, 110902 (2019).
[40] M. A. Caro, S. Schulz, and E. P. O'Reilly, Phys. Rev. B 88, 214103 (2013).
[41] C. Y. Ho, C. P. Liu, Y. C. Chen, Z. Q. Huang, F. C. Chuang, and K. M. Yu, Phys. Rev. Materials 3, 074605 (2019).
[42] R. R. Pelá, C. Caetano, M. Marques, L. G. Ferreira, J. Furthmüller, Appl. Phys. Lett. 98, 151907 (2011).
[43] M. Yamada, T. Mitani, Y. Narukawa, S. Shioji, I. Niki, S. Sonobe, K. Deguchi, M. Sano, and T. Mukai, Jpn. J. Appl. Phys., 41:L1431 (2002).
[44] V. Awasthi, S. K. Pandey, S. Verma, and S. Mukherjee, J. Lumin. 180, 07010 (2016).
[45] P. T. Barletta, E. A. Berkman, B. F. Moody, N. A. El-Masry, A. M. Emara, M. J. Reed, and S. M. Bedair, Appl. Phys. Lett., 90:151109 (2007).
[46] N. A. El-Masry, E. L. Piner, S. X. Liu, and S. M. Bedair, Appl. Phys. Lett. 72, 40 (1998).
[47] I. Sayed and S. M. Bedair, IEEE J. Photovolt. 9 (2019).
[48] M. R. Krames, O. B. Shchekin, R. Mueller-Mach, G. O. Mueller, L. Zhou, G. Harbers, and M. G. Craford, J. Disp. Technol., 3:160 (2007).
[49] A. Assali , M. Bouslama, H. Abid, S. Zerroug, M. Ghaffour, F. Saidi, L. Bouzaiene, K. Boulenouar, Mater. Sci. Semicond. Process. 36 (2015).
[50] F. Mouhat and F. X. Coudert, Phys. Rev. B 90, 224104 (2014).
[51] M. J. Mehl, J. E. Osburn, D. A. Papaconstantopoulos, and B. M. Klein, Phys. Rev. B 41, 10311 (1990).
[52] S. F. Pugh, Philos. Mag. 45 (1954).
[53] G. N. Greaves, A. Greer, R. Lakes, and T. Rouxel, Nat. Mater. 10, (2011).
[54] S.I. Ranganathan and M. Ostoja-Starzewski, Phys. Rev. Lett. 101, 055504 (2008).
[55] M. de Jong, W. Chen, T. Angsten, A. Jain, R. Notestine, A. Gamst, M. Sluiter, C. K. Ande, S. van der Zwaag, J. J. Plata, C. Toher, S. Curtarolo, G. Ceder, K. A. Persson, and Mark Asta, Sci. Data 2 (2015).
[56] R. D. King-Smith, D. Vanderbilt, Phys. Rev. B 47, 1651 (1993).
[57] R. Resta, Rev. Mod. Phys. 66, 899 (1993).
[58] R. Resta and D. Vanderbilt, Top. Appl. Phys. 105 (2007).

[59] M. V. Berry, Proc. R. Soc. London Ser. A 392, 45 (1984).
[60] F. Bernardini, V. Fiorentini, and D. Vanderbilt, Phys. Rev. B 63, 193201 (2001).
[61] A. D. Corso, M. Posternak, R. Resta, and A. Baldereschi, Phys. Rev. B 50, 10715 (1994).
[62] J. Lähnemann, O. Brandt, U. Jahn, C. Pfüller, C. Roder, P. Dogan, F. Grosse, A. Belabbes, F. Bechstedt, A. Trampert, and L. Geelhaar, Phys. Rev. B 86, 081302 (2012).
[63] V. Fiorentini, F. Bernardini, F. D. Sala, A. Di Carlo, and P. Lugli, Phys. Rev. B 60, 8849 (1999).
[64] N. Grandjean, J. Massies, and M. Leroux, Appl. Phys. Lett. 74, 2361 (1999).
[65] T. Takeuchi, S. Sota, M. Katsuragawa, M. Komori, H. Takeuchi, H. Amano, and I. Akasaki, Jpn. J. Appl. Phys., 36:L382 (1997).
[66] E. Kioupakis, Q. Yan, and C. G. Van de Walle, Appl. Phys. Lett. 101, 231107 (2012).
[67] M.-H. Kim, M. F. Schubert, Q. Dai, J. K. Kim, E. F. Schubert, J. Piprek, and Y. Park. Appl. Phys. Lett. 91, 183507 (2007).
[68] J. J. Wierer, A. J. Fischer, and D. D. Koleske, Appl. Phys. Lett. 96, 051107 (2010).
[69] Z. Q. Li, M. Lestradet, Y. G. Xiao, and S. Li, Phys. Status Solidi A 208, 928 (2011).
[70] M. A. Caro, S. Schulz, S. B. Healy, and E. P. O'Reilly, J. Appl. Phys. 109, 084110 (2011).

## Acknowledgement

This research was supported by the Directorate General for Scientific Research and Technological Development DGRSDT – MESRS, Algeria.

### Author Contributions

S.M conceived and proposed the research idea. A.Be and S.M performed the simulation for InGaN and CdZnO, respectively. A.Be wrote the manuscript, with assistance from H.A, E.A, and S.M. A.Bo supervised the work. All authors contributed to the scientific discussion.

## Competing Interests

The authors declare that there are no competing interests.